Geomechanics and Engineering, *Vol. 24, No. 4 (2021) 307-321*
DOI: https://doi.org/10.12989/gae.2021.24.4.307

Theoretical model for the shear strength of rock discontinuities with non-associated flow laws

Rubén Galindo*[1], José L. Andrés[1], Antonio Lara[1], Bin Xu[2], Zhigang Cao[2] and Yuanqiang Cai[2]

[1]Department of Geotechnical Engineering, Universidad Politécnica de Madrid, C/ Profesor Aranguren s/n 28040 Madrid, Spain
[2]Department of Civil Engineering, College of Civil Engineering and Architecture, Zhejiang University, Hangzhou 310058, PR China

(Received May 6, 2020, Revised January 26, 2021, Accepted January 28, 2021)

Abstract. In an earlier publication (Serrano *et al.* 2014), the theoretical basis for evaluating the shear strength in rock joints was presented and used to derive an equation that governs the relationship between tangential and normal stresses on the joint during slippage between the joint faces.
In this paper, the theoretical equation is applied to two non-linear failure criteria by using non-associated flow laws, including the modified Hoek and Brown and modified Mohr-Coulomb equations.
The theoretical model considers the geometric dilatancy, the instantaneous friction angle, and a parameter that considers joint surface roughness as dependent variables. This model uses a similar equation structure to the empirical law that was proposed by Barton in 1973. However, a good correlation with the empirical values and, therefore, Barton's equation is necessary to incorporate a non-associated flow law that governs breakage processes in rock masses and becomes more significant in highly fractured media, which can be induced in a rock joint. A linear law of dilatancy is used to assess the importance of the non-associated flow to obtain very close values for different roughness states, so the best results are obtained for null material dilatancy, which considers significant changes that correspond to soft rock masses or altered zones of weakness.

Keywords: rock joint; shear strength; theoretical model; dilatancy; non-linear criterion; non-associated flow law

1. Introduction

Determining the shear strength of rock joints requires understanding the relationship between the mean normal stress on the rupture plane (mid-plane of the discontinuity) and the mean tangential stress that is produced by the slippage between the two rock faces.

In the case of rock joints, the rock contact breaks and, as in any process that is related to the breakage mechanics of rock masses, a good approximation of the strength phenomena involves adequate knowledge of the strength laws of such rock masses. In this regard, adequate research must be conducted in the framework of well-established failure criteria to study rock masses.

Furthermore, adequately predicting breakage phenomena when the deviator load becomes significant (such as rock joints where the shear load that defines breakage on the median plane of the discontinuity is determined for a given normal load level in this plane) must consider the dilatancy of the material, whose influence is well known in rock materials (Hoek and Brown 1997, Fairhurst 2003, Alejano and Alonso 2005).

Both a suitable failure criterion and the dilatancy law were incorporated into a previously established theoretical model (Serrano *et al.* 2014) to better predict and approximate experimental results, with a particular formulation established by Barton (1973).

Pioneering works regarding the evolution of the study of rock joints include the following. Patton (1967) proposed a formulation that was based on a saw-tooth pattern and was based on tests that were performed on artificially created joints in gypsum material. Ladanyi and Archambault (1969) and Jaeger (1971) used more sophisticated adjustment laws. However, Barton (1973) had the most success by incorporating an empirical formula that considered the effects of joint roughness and dependence on the load level into his dilatancy prediction study.

More complex empirical models then began to appear. Some models compared the angles that defined the surface roughness by the normal stress (Schneider 1976). Heuze and Babour (1982) introduced a three-parameter model to predict the dilatancy that is produced in rock joints by empirically identifying a critical point beyond which no dilatancy exists. Additionally, Leichnitz (1985) developed a model that could consider rock fractures that were produced by nonlinear behaviour in the material based on experimental results from sandstone.

Plesha (1987) studied a degradation factor for roughness from the saw-tooth roughness model. Qiu *et al.* (1993) revised Plesha's model by considering sinusoidal instead of saw-tooth roughness. Saeb and Amadei (1992) conducted a similar study based on an empirical ratio of the dilatancy factor, which was given by Ladanyi and Archambault (1969). Recently, other investigations of the degradation of roughness in contacts between joint faces were performed. Belem (2016) proposed different quantitative parameters for the characterization of the primary roughness which are

*Corresponding author, Professor
E-mail: rubenangel.galindo@upm.es

ISSN: 2005-307X (Print), 2092-6219 (Online)

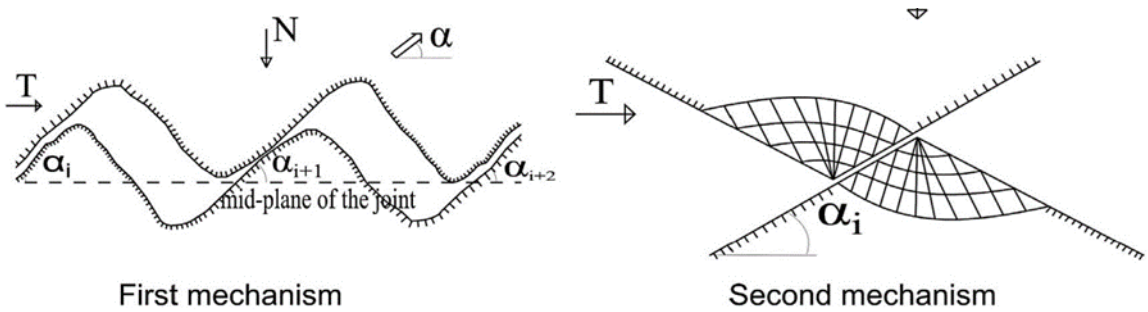

Fig. 1 First failure mechanism (slippage) and second failure mechanism (plastification of the contacts)

mostly the anisotropic properties of rock surface morphology at various scales: coefficient and degree of apparent structural anisotropy of surface; coefficient and degree of real structural anisotropy of surface; surface anisotropy function and degree of surface waviness. The proposed quantitative parameters allows their application at both lab and field scales. Zhang *et al.* (2017) used a 3D optical scanner to measure the joint morphology and performed direct shear tests under constant normal load conditions on artificial rock joints with different morphology. As the normal stress increases, the percentage of shear-off rises gradually before approaching a stable level, whereas dilation consistently decreases.

Gens *et al.* (1990) proposed an elastoplastic constitutive model to describe the three-dimensional behaviours of fractures. Grasselli (2003), Belem (2007) and Samadhiya *et al.* (2008) formulated parameter models that considered the three-dimensional natures of joint surfaces. More reciently, Hu and Lin (2018) analyzed the shear strength on joint asperities and adopted a hyperbolic function to describe the degradation of friction for different normal stress levels. Furthermore, the proposed model avoids direct connection to the surface morphology, which is convenient for practical use. Lin *et al.* (2020) applied the nonlinear shear strength model, JRC-JCS model, to study the overall shear resistance of the joint under four nonuniform distribution patterns of normal stress. The results show that when the normal stress is distributed in a nonuniform way, the shear resistance provided by rock joint as a whole decreases with the increase of the normal stress distribution interval. Chong *et al.* (2020) performed experimental studies using the quasi-static resonant column testing device on regularly jointed disc column specimens for three different materials. The wave velocities of the specimens are obtained under various normal stress levels. The normal and shear joint stiffness are calculated from the experimental results using an equivalent continuum model and used as input parameters for numerical analysis. Based on the calibrated jointed rock model, the numerical and experimental results are compared.

Among the existing models, Barton's empirical method (1973) is the most widely used in practice. This method is based on the selection of a joint roughness coefficient (JRC), for which various approaches have been proposed to relate this value to the morphologies of the profiles that it defines; these approaches have also evaluated the use of fractal analysis (Lee *et al.* 1990, Huang *et al.* 1992, Muralha 1995, Xie *et al.* 1999).

Asadollahi (2009), in an application to stability analysis of a single three dimensional rock block, introduced a modification of Barton's original shear failure criterion, which was based on limitations in Barton's criterion concerning the estimation of the peak displacement or post-peak shear strength. Zhao *et al.* (2020) also investigated the stability of a three-dimensional (3D) wedge under the pseudo-static action of an earthquake based on the nonlinear Barton-Bandis failure criterion. The parametric analyses showed that the stability coefficient and the instability mode of the wedge depend on the mechanical parameter of the rock mass; in particular, the friction angle of the rock and the roughness coefficient of the structure surface JRC are sensitive to stability.

However, the theoretical basis of the shear strength of rock joints was established by Serrano *et al.* (2014), who developed a theoretical model that could capture the primary mathematical structure of Barton's equation and the dependence of the variables that are used in the description of this equation.

The aim of this article is to apply this theoretical formulation (2014) to more precisely define the shear strength of rock joints in accordance with known experimental results. We must use appropriate failure criteria, which must be nonlinear, and consider the dilatancy of rocks by a non-associated flow law.

Thus, two well-established nonlinear failure criteria are used: the modified Hoek and Brown criterion (Hoek *et al.* 2002) and the modified Mohr-Coulomb criterion (Singh *et al.* 2011, Singh and Singh 2012). Additionally, the effect of the material's dilatancy is considered by using a linear variation law with respect to the instantaneous friction angle so that model considers both the geometrical dilatancy from the breaking of contacts according to planes of weakness on the asperities of the roughness and the material's dilatancy by using a non-associated flow law.

However, the scope of the presented mathematical formulation considers both the evaluation of a geometric parameter of real roughness for the considered problem and the height and length of each joint's roughness in laboratory samples. Therefore, scaling the results of these laboratory samples to joints of different sizes is not the subject of this investigation.

2. Theoretical model

Two failure mechanisms occur when contact occurs

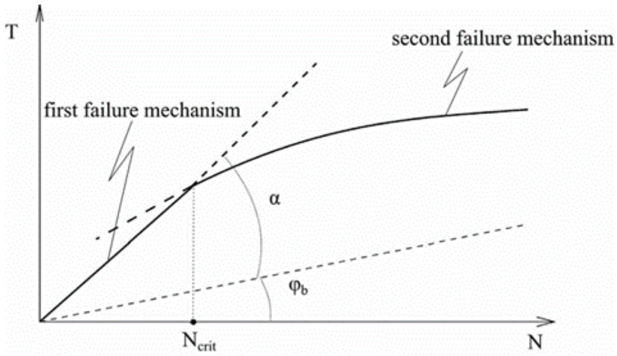

Fig. 2 Peak shear strength governing law

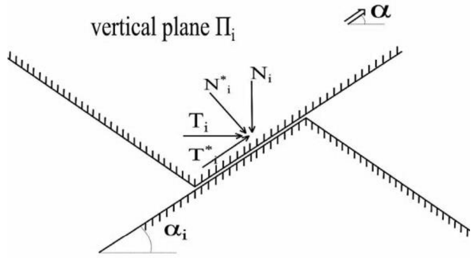

Fig. 3 Contact forces according to the first failure mechanism

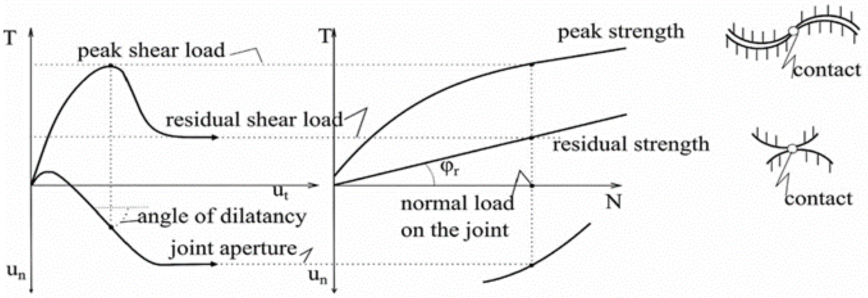

Fig. 4 Influence of surface roughness smoothing along the opening of the joint

through surface roughness. In the first mechanism, the joint slips and forms an angle α with the mid-plane of the joint (Fig. 1); this mechanism is used for low normal loads. In the second mechanism, the roughness is plastified and breaks (Fig. 1), which is used for high normal exterior loads.

The critical normal load N_{crit} discriminates between both mechanisms. Failure occurs through the first mechanism for normal stresses below this critical load, while the second mechanism applies to loads above the critical level (Fig. 2).

2.1 First mechanism analysis

The *i*-th contact between the roughness areas is considered according to the joint profile. The tangential plane in the *i*-th contact is assumed to form the maximum angle α_i with the mid-plane of the joint in a section over the vertical plane Π_i, which is perpendicular to the mid-plane in the direction of the shear load. Slippage is produced when

$$\frac{T_i}{N_i} = tan(\varphi_b + \alpha_i) = tan(\varphi_p)_i$$

where φ_b is the basic friction angle of the material and T_i and N_i are the tangential and normal force in the direction of the mid-plane, respectively (Fig. 3). The tangential and normal force in the direction of the tangential plane in the *i*-th contact are expressed through T_i^* and N_i^*. The notation $(\varphi_p)_i$ (peak friction angle) is used for $\varphi_b + \alpha_i$.

If these arguments are extended to the *n* contacts between the joint faces and a uniform distribution of force per unit of surface is assumed, we can obtain the joint shear strength governing law according to the first mechanism:

$$\frac{\tau}{\sigma_n} = tan(\varphi_b + \alpha) \tag{1}$$

The practical way to approach this first slippage mechanism includes the assumption of a constant average slope for all contacts. Thus, we suppose that slippage is produced along a plane that is formed by angle α and the mid-plane according to equation (1). Thus, movement between the joint walls is produced with constant dilatancy according to this angle; this phenomenon is defined as geometric dilatancy because it is produced by the geometry of the joint surface.

When analysing this mechanism in terms of more realistic surfaces, the above-described equations are verified in each equilibrium state by varying the angle of the slope at the contact along the joint opening. This condition supposes variation in the strength law of the first mechanism with the relative displacement that is produced between the joint faces. This geometrical configuration, which is mainly produced from damage to the asperities, can explain strength reductions such that when failure via slippage occurs with a constant normal load, the strength against the tangential stress is lower because the contact angle is smaller in a higher position. Thus, for joints in which this first mechanism of failure via slippage is produced, the space that constitutes the height of the contacts changes from the peak strength to the basic or residual distance. At this point, the geometric dilatancy is null (Fig. 4). However, from a practical perspective, we can consider the slope α_i for each roughness at a constant value and the value of the average contact angle θ_i.

2.2 Analysis of the second mechanism

The interaction between the edges of a joint consists of a large number of contact points such that the force is transmitted through these points. Failure can occur when the load on each contact is sufficiently high (Fig. 1). This situation can be mathematically modelled by supposing that the geometry of the joint can be defined by a particular surface roughness profile and adopting some hypotheses, as indicated below.

The rock matrix obeys the shear strength governing law: $\tau = \tau(\sigma)$.

When failure is produced by this mechanism, the joint moves with a dilatancy that is defined by the angle δ. The fracture surface for each given roughness is flat (Fig. 5).

Another hypothesis is that the fracture area a_i of each contact depends on the dilatancy angle δ according to a particular angle $a_i(\delta)$.

One last hypothesis is used: rupture is produced for a dilatancy angle δ that minimises the total shearing force T of the failure for a certain constant normal load N over the joint. This condition can be mathematically expressed as

$$\left(\frac{\partial T}{\partial \delta}\right)_{N=const} = 0 \tag{2}$$

where $T = \sum T_i$.

Based on these hypotheses, the joint shear strength governing law can be mathematically deduced to relate the joint-plane stresses τ and the normal stress σ_n for the second failure mechanism as follows (Serrano *et al.* 2014):

$$\frac{\tau}{\sigma_n} = \frac{T}{N} = tan(\rho + \kappa_m + \delta) \tag{3}$$

where δ is the dilatancy angle at failure, ρ is the instantaneous friction angle and κ_m is the angle that represents the reduction in the area of contact in the joint and should be obtained from the geometrical properties of the different roughness values (Fig. 5) such that for one *i*-th contact (Serrano *et al.* 2014):

$$\frac{1}{tan\,\kappa_i} = \frac{-1}{a_i}\frac{da_i}{d\delta} \tag{4}$$

3. Barton's empirical model (1973)

Barton (1973) experimentally studied the law governing the shear strength of a rock joint from the following empirical equations:

$$\frac{\tau}{\sigma_n} = tan(\varphi_b + \delta + f) = tan\,\varphi_p \tag{5}$$

$$\varphi_p - \varphi_b = JRC\,log\frac{JCS}{\sigma_n} \tag{6}$$

where

τ and σ_n are the stresses at the onset of failure according to the tangential and normal angles, respectively,

φ_b is the basic friction angle of the "healthy" joint wall,

δ is the dilatancy angle at the onset of joint movement,

f is a parameter that depends on the roughness,

JRC is the joint roughness coefficient, which depends on surface roughness, and

JCS represents the joint wall compressive strength of the rock wall.

Eq. (6) is restricted to σ_c/σ_n values that are greater than 50 to 100 and that have a constant and independent friction angle from the load of

$$\varphi_p = \varphi_b + 1.7JRC \tag{7}$$

When the joint surfaces are altered, the roughness is smoothed and dilatancy disappears. In this case, the residual friction angle φ_r is reached and $\varphi_b = \varphi_r$ (in principle; throughout this text, this relationship is considered the basic friction angle; however, this angle coincides with the residual value when joint surface alteration exists).

However, a scale effect can be considered for tests of the JRC and JCS values when using correction equations (Barton and Bandis 1982).

Eq. (5) depends on the basic friction angle of the joint wall (φ_b), the dilatancy angle (δ) and the roughness characteristics (f). In the above theoretical formula (equation (3)), the shear strength of the joint is a function of the instantaneous angle of roughness (ρ), the geometric dilatancy (δ) and the degree of reduction in the contact area and depends on geometric properties that define the roughness (κ_m). The observed similarity is not random but rather the result of an adequate consideration of the factors that contribute to joint failure through the presented hypothesis and theoretical formulation.

4. Influence of roughness geometric factors

The influences of the surface roughness shape and geometry on the second failure mechanism are clearly shown in this theoretical formulation by using the reduction in the contact area κ_m. In Barton's empirical formula, the influence of the surface roughness on the strength law was articulated with the JRC index, which in its initial formation was determined according to the similarity of the real joint to standard roughness profiles. Subsequently, statistical and fractal methods were suggested that supported correlations of this index with the parameters of the joint roughness

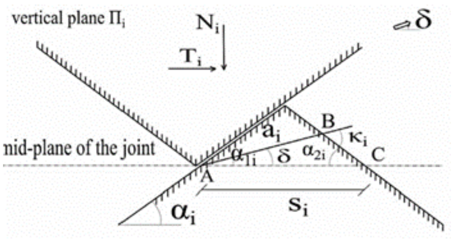

(a)

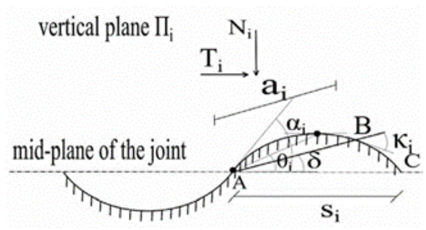

(b)

Fig. 5 (a) Rupture of a saw-tooth joint in contact i and (b) linear surface roughness according to the circumference arcs in contact i

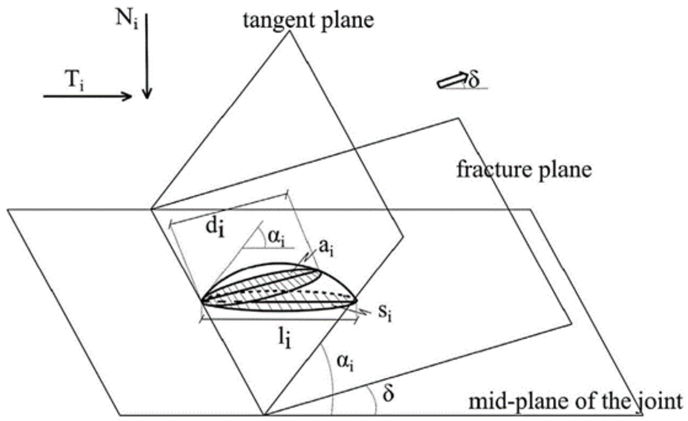

Fig. 6 Three-dimensional surface roughness according to the spherical caps in contact i

profile to improve the objectivity of the estimate (Lee *et al.* 1990, Huang *et al.* 1992, Muralha 1995, Xie *et al.* 1999).

A simple and representative manner to represent the roughness of a rock surface can be constructed from the height h_i and amplitude b_i for each roughness such that the average contact angle of the irregularity θ_i may be represented as $tan\theta_i = 2h_i/b_i$.

A simplified study consists of the supposition of simple shapes for irregularities, including saw-teeth or softened curves that form circumference arcs, such that the roughness can be determined from a single parameter: the slope angle for each roughness.

In the theoretical model for the second mechanism, the joint geometry influences the parameter that is defined as κ_m. The dependence κ_i of the angle of reduction for each contact can be deduced for the various geometries that are used to define the joint profiles (Serrano *et al.* 2014).

The use of a saw-tooth joint profile assumes work in a plane deformation problem. For contact i, angles α_{1i} and α_{2i} are formed, as shown in Fig. 5(a):

$$\kappa_i = \alpha_{2i} + \delta \tag{8}$$

The use of circumference arcs for joint profiles is also present in plane deformation. Angle α_i corresponds to the tangent plane in contact *i* to create an ideal and symmetrical surface roughness geometry with regard to the mid-plane (Fig. 5(b)):

$$\kappa_i = \alpha_i - \delta \tag{9}$$

The relationship between the angle in the contact and the average irregularity angle is direct and is shown by $\alpha_i = 2\theta_i$.

For a better approach to study real joints, we should consider that the surface roughness has a three-dimensional nature whose geometry consists of spherical caps. In this case, the contact area between the joint faces is lower than that in plane deformation models: specifically, the intersections are circular. Fig. 6 represents the evaluated geometry for irregularities. As shown throughout the text, angle α_i serves as the roughness parameter and forms the tangent to the contact in the mid-plane of the joint:

$$tan\,\kappa_i = \frac{tan(\alpha_i - \delta)}{2} \tag{10}$$

As with the prior case, using the average roughness angle $\theta_i = \alpha_i/2$ can be more practical.

Comparing predictions from the theoretical model with the Barton criteria requires relating the JRC with the geometric variable α_i (or θ_i), which is used to define the roughness.

Thus, to characterise the geometry of irregularities with softened profiles, we propose characterising the fractal dimension of the joints with a circumference arc generator that depends on the already-defined average contact angle θ with regard to the mid-plane (Fig. 6) according to the surface roughness geometry of the circumference arcs. For this model, the following fractal dimension is obtained Serrano *et al.* (2014):

$$D_b = \frac{ln\,3}{ln\left(2 + \frac{sin2\,\theta}{2\theta}\right)} \tag{11}$$

The correlation between the JRC and the fractal dimension of the established model can be obtained with the statistical empirical ratio that was used by Tse and

Cruden (1979). The empirical relationship between the JRC value and the fractal dimension for the fractal model in Fig. 6 can be expressed by using the following equation (Serrano *et al.* 2014):

$$JRC = 8.0011\, ln(D_b - 1) + 41.8964 \qquad (12)$$

5. Influence of the intrinsic resistance law of the rock on the contacts

5.1 Modified Hoek and Brown failure criterion

The modified Hoek-Brown criterion (Hoek *et al.* 2002) is as follows:

$$\frac{\sigma_1 - \sigma_3}{\sigma_c} = \left(m\frac{\sigma_3}{\sigma_c} + s\right)^n \qquad (13)$$

where σ_1 is the major principal stress at failure; σ_3 is the minor principal stress; σ_c is the uniaxial compressive strength of the rock matrix; and *m* and *s* are constants that depend on the characteristics of the rock mass, its degree of fracturing and the disturbance factor *D*. The value of the exponent *n* also generally depends on the degree of fracturing by means of the Geological Strength Index (GSI). Its equation is as follows (Hoek *et al.* 2002):

$$n = \frac{1}{2} + \frac{1}{6}\left(e^{-GSI/15} - e^{-20/3}\right) \qquad (14)$$

For rock joints, the disturbance factor *D* can be conveniently chosen to represent the conditions of alteration along the surface sides of the joint. The condition to estimate this alteration is expressed by Eq. (43) below.

The expression for the modified Hoek-Brown failure criterion, which involves Lambe's variables for plane strain analysis, ($p=(\sigma_1 + \sigma_3)/2$ and $q=(\sigma_1 - \sigma_3)/2$), permits a simplified and normalized treatment of the rock mass failure phenomena. With these variables, the modified Hoek-Brown failure criterion is expressed as follows (Serrano *et al.* 2000):

$$\frac{p}{\beta_n} + \zeta_n = \left[1 + (1-n)\left(\frac{q}{\beta_n}\right)^k\right]\frac{q}{\beta_n} \qquad (15)$$

where *k,* β_n and ζ_n are constants that represent the rock mass and depend on *n*, *m*, *s* and σ_c as follows:

$$k = (1-n)/n;\ \beta_n = A_n\sigma_c;\ \zeta_n = s/(mA_n) \qquad (16)$$

where $A_n^k = m(1-n)/2^{1/n}$.

The failure above the Mohr circles, $\tau = \tau\,(\sigma)$, is defined by (Fig. 7):

$$\tau = q\cos\psi \qquad (17)$$

$$\sigma = p - q\sin\psi \qquad (18)$$

where ψ is the dilatancy angle, which marks the breaking point of the failure criterion on Mohr's circle.

The important concept of the instantaneous friction angle is defined after Serrano and Olalla (1994):

$$\sin\rho = \frac{dq}{dp} \qquad (19)$$

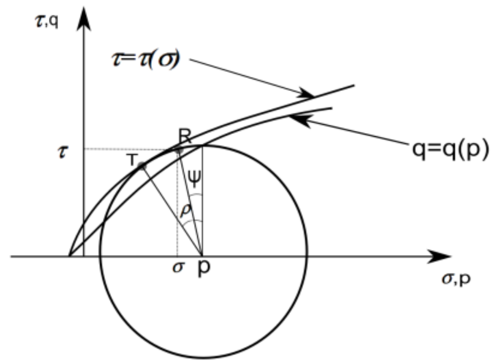

Fig. 7 Mohr's circle of stresses and the stress on the failure plane

According to Eq. (15),

$$\sin\rho = \frac{dq}{dp} = \frac{1}{1 + k\left(\frac{q}{\beta_n}\right)^k} \qquad (20)$$

The parametric equations are obtained for the criterion with Lambe's variables, using (15) and (20):

$$q^* \equiv \frac{q}{\beta_n} = \left[\frac{1 - \sin\rho}{k\sin\rho}\right]^{1/k} \qquad (21)$$

$$p_0^* \equiv \frac{p}{\beta_n} + \zeta_n = n\left[\frac{1 + k\sin\rho}{\sin\rho}\right]\left[\frac{1 - \sin\rho}{k\sin\rho}\right]^{1/k} \qquad (22)$$

The parametric expressions of the failure stresses on Mohr's circle for the generalized Hoek-Brown failure criterion (2002) under a non-associated flow law can be obtained by considering (17), (18), (21) and (22):

$$\tau^* \equiv \frac{\tau}{\beta_n} = \left[\frac{1 - \sin\rho}{k\sin\rho}\right]^{1/k}\cos\psi \qquad (23)$$

$$\sigma_0^* \equiv \frac{\sigma}{\beta_n} + \zeta_n = \left(\frac{1 - \sin\rho}{k\sin\rho}\right)^{1/k}\left[n\left(\frac{1 + k\sin\rho}{\sin\rho}\right) - \sin\psi\right] \qquad (24)$$

5.2 Modified Mohr-Coulomb failure criterion

A non-linear strength criterion of a rock mass was suggested by Singh *et al.* (2011) and Singh and Singh (2012) as follows:

$$\sigma_1 - \sigma_3 = \sigma_{cj} + 2\frac{\sin\varphi_j}{1 - \sin\varphi_j}\sigma_3 - \frac{\sin\varphi_j}{1 - \sin\varphi_j}\frac{{\sigma_3}^2}{\sigma_c} \qquad (25)$$

If $\sigma_3 > \sigma_c$, then $\sigma_1 - \sigma_3 = \sigma_{cj} + \frac{\sin\varphi_j}{1-\sin\varphi_j}\sigma_c$. That is, when $(\sigma_1 - \sigma_3)$ reaches its maximum value in (25), then this value is considered constant $(\sigma_1 - \sigma_3)$ and equal to that maximum value:

σ_3 and σ_1 are the effective minor and major principal stresses at failure,

σ_c is the uniaxial compressive strength of the intact rock,

σ_{cj} is the rock mass strength, and

φ_j is the friction angle, which is obtained by conducting triaxial strength tests on rock specimens at low confining pressures ($\sigma_3 \to 0$).

Eq. (25) can be expressed in a normalized form by dividing by σ_c:

$$\sigma_1{}^* - \sigma_3{}^* = \frac{\sigma_{cj}}{\sigma_c} + 2\frac{\sin\varphi_j}{1-\sin\varphi_j}\sigma_3{}^* - \frac{\sin\varphi_j}{1-\sin\varphi_j}(\sigma_3{}^*)^2 \quad (26)$$

Eq. (26) can be written in a simpler form for all rocks:

$$\sigma_1{}^* - \sigma_3{}^* = r + 2n_j\sigma_3{}^* - n_j(\sigma_3{}^*)^2 \quad (27)$$

where $n_j = \frac{\sin\varphi_j}{1-\sin\varphi_j}$ and $r = \frac{\sigma_{cj}}{\sigma_c}$.

By using the Lambe parameters, $p = (\sigma_1+\sigma_3)/2$ and $q = (\sigma_1-\sigma_3)/2$, the modified Mohr-Coulomb criterion can be expressed as follows:

$$2q^* = r + 2n_j(p^*-q^*) - n_j(p^*-q^*)^2 \quad (28)$$

$$2p^* = r + 2(n_j+1)(p^*-q^*) - n_j(p^*-q^*)^2 \quad (29)$$

By using Eqs. (28) and (29) and for $t^* = \sigma_3{}^*$, the following expressions can be obtained:

$$2q^* = r + n_j - \frac{1}{n_j}\left(\frac{\sin\rho}{1-\sin\rho}\right)^2 \quad (30)$$

$$2p^* = 2 + r + n_j - \frac{2}{n_j}\left(\frac{\sin\rho}{1-\sin\rho}\right) - \frac{1}{n_j}\left(\frac{\sin\rho}{1-\sin\rho}\right)^2 \quad (31)$$

$$\sin\rho = \frac{n_j(1-t^*)}{1+n_j(1-t^*)} \quad (32)$$

For a realistic prediction of strength, the criterion parameters (r and n_j) must be assessed with good accuracy. Estimating the value of n_j requires the parameter φ_j, which can be obtained as discussed by Singh and Singh (2012):

$$n_j = n_0 + (1-r)$$
$$n_0 = \frac{\sin\varphi}{1-\sin\varphi} \quad (33)$$

where φ is the friction angle, which is obtained by conducting triaxial strength tests on intact rock at low confining pressures ($\sigma_3 \to 0$). Therefore,

$$\sin\varphi_j = \frac{1-r+n_0}{2-r+n_0} \quad (34)$$

The other parameter (r) involves estimating σ_{cj}.

From (16), (17), (30), (31) and (32), the parametric expressions for failure on Mohr's circle for the generalized Mohr-Coulomb failure criterion under a non-associated flow law are

$$\tau^* = \frac{1}{2}\left[r + n_j - \frac{1}{n_j}\left(\frac{\sin\rho}{1-\sin\rho}\right)^2\right]\cos\psi \quad (35)$$

$$\sigma^* = \frac{1}{2n_j}\left(\frac{\sin\rho}{1-\sin\rho}\right)^2(-1+\sin\psi) - \frac{1}{n_j}\left(\frac{\sin\rho}{1-\sin\rho}\right) + \frac{r+n_j}{2}(1-\sin\psi) + 1 \quad (36)$$

5.3 Non-associated flow law

The critical angle ($\sin\rho_{crit}$) is defined as the instantaneous friction angle from which the rock mass stops being positively dilatant. After this point, the dilatancy is null and no changes occur in the volume during the plastification of the rock mass. From this definition, the critical angle can be obtained based on the expressions from (17) and (18), by considering the critical ratio (σ_1/σ_3). For the original Hoek and Brown criterion and modified Mohr-Coulomb criterion, we can obtain explicit expressions by means of following equations.

For the original Hoek and Brown criterion:

$$\sin\rho_{crit} = \frac{\frac{\sigma_1}{\sigma_3} - 1}{\left(\frac{\sigma_1}{\sigma_3}+1\right) + 2\sqrt{1 + \frac{\zeta}{2}\left(\frac{\sigma_1}{\sigma_3}-1\right)^2}}$$

For the modified Mohr-Coulomb criterion:

$$\sin\rho_{crit} = \frac{1+A}{2+A+B};$$
$$A = \sqrt{1 - n_j(1+B)\left[2 + (r+n_j)(1-B)\right]};B = \frac{\frac{\sigma_1}{\sigma_3}+1}{\frac{\sigma_1}{\sigma_3}-1}$$

This critical angle ρ_{crit} presents a variable value that approximately lies between 0º and 30º and depends on the values of the parameters. According to the expression of the original Hoek and Brown criterion, the latter corresponds to the matrix rock ($\sigma_1 = 5\sigma_3$), which reaches 0º when $\sigma_1 = \sigma_3$ for rock masses.

The maximum dilatancy ($\sin\psi_{max}$), which is defined as the maximum angle of dilatancy, is produced when the rock mass undergoes simple traction. The failure lines form the angle ($\pi/4 - \psi/2$) with the major principal strain (and with σ_1 because this factor refers to coaxial materials).

In the event that a rock sample undergoes a simple traction test, failure is always produced in a perpendicular direction to the minor principal stress such that the failure lines form an angle of $\pi/2$ with the major principal strain, whereby the angle that corresponds to the maximum dilatancy reaches a value of $\pi/2$.

Under this consideration, a linear flow law was tested in this paper. The mathematical expression of this flow law is

$$\sin\psi = \frac{\sin\psi_{max}}{1-\sin\rho_{crit}}(\sin\rho - \sin\rho_{crit}) \;\; if \;\; \rho < \rho_{crit} \to \psi = 0$$

The proposed flow law follows the recommendations by Veermer and De Borst (1984) such that it is a function of the internal friction angle (variable depending on the stress conditions) and the critical material angle. Thus, the linear dilatancy law can be expressed as follows:

$$\sin\psi = E\sin\rho - F \quad (37)$$

where E and F are non-negative constants such that $E \leq 2$, $F \leq 1$ and $E\text{-}F \leq 1$.

The case of E=1 and F=0 corresponds to the associated flow law, whereas E=F=0 implies a null dilatancy.

Thus, dilatancy laws according to Eq. (37) for different values of E and F have been used for this search.

The inferred state at a rock joint corresponds to a rock's altered quality (indicating less dilatancy than expected and therefore worse strength compared to a healthy rock mass). Archambault *et al.* (1993) observed that when increasing the scale of the analysis, the peak strength decreases, the residual strength is maintained and thus the dilatancy remains lower, so the material begins to expand to a higher level of plastic deformation. If we consider the quality index to account for the effect of scale, these observations are consistent with the proposals of Hoek and Brown (1998), which indicate that the difference between the peak and residual strength is higher at a smaller scale (i.e., more geotechnical quality).

In this respect and with regard to the flow rule, some works (Hoek and Brown 1997, Fairhurst 2003) demonstrated the need to use a non-associated flow rule and, in particular, adopt null dilatancy for soft rock masses, which corresponds to deformation over a constant volume. Thus, the results shown in the following section for the theoretical model of the shear strength of discontinuities are very close to the experimental values when adopting values of E=F=0 in (37), i.e., zero dilatancy.

6. Application of the theoretical model with a non-associated flow law

The second shear stress mechanism is associated with the failure of roughness and thus requires incorporating an intrinsic strength criterion with which to model this failure. Studies of rocks require nonlinear failure criteria to consider the influences of confining pressures on the shear resistance. The use of this analysis criterion provides a basis for comparison with the empirical Barton model.

A modified Hoek and Brown failure criterion and a modified Mohr-Coulomb criterion were applied by considering a non-associated flow law in both cases.

6.1 Modified Hoek and Brown failure criterion

The modified Hoek and Brown failure criterion (Hoek *et al.* 2002) with non-associated flow can be expressed in a parametric form with the instantaneous friction angle as the variable (Serrano and Olalla 1994) according to Eqs. (23) and (24). In such expressions, the subscript i is used when applied to one asperity, and the subscript r is used to indicate variables in the failure plane.

The expressions that relate the forces on the global axes and those of the failure plane satisfy the following:

$$N_i = a_{ir}(\sigma_{ri} \cos\delta - \tau_{ri} \sin\delta) \tag{38}$$

$$T_i = a_{ir}(\sigma_{ri} \sin\delta + \tau_{ri} \cos\delta) \tag{39}$$

Based on the above expressions, we can obtain specific equations for each type of modelled roughness. However, the most realistic case is that of geometrical modelling with spherical caps. In this case,

$$a_{ir} = a_i \frac{\sin^2(\alpha_i - \delta)}{\sin^2 \alpha_i} \tag{40}$$

Substituting equations (23), (24) and (40) into equations (38) and (39) for the modified Hoek and Brown failure produces the following:

$$\begin{aligned} N_i &= \beta_n a_i \frac{\sin^2(\alpha_i - \delta)}{\sin^2 \alpha_i} \left[\left(n \left[\frac{1 + k \sin\rho}{\sin\rho} \right] \left[\frac{1 - \sin\rho}{k \sin\rho} \right]^{1/k} \right.\right. \\ &\left.\left. - \zeta_n - \left[\frac{1 - \sin\rho}{k \sin\rho} \right]^{1/k} \sin\psi \right) \cos\delta - \left[\frac{1 - \sin\rho}{k \sin\rho} \right]^{1/k} \cos\psi \sin\delta \right] \end{aligned} \tag{41}$$

$$\begin{aligned} T_i &= \beta_n a_i \frac{\sin^2(\alpha_i - \delta)}{\sin^2 \alpha_i} \left[\left(n \left[\frac{1 + k \sin\rho}{\sin\rho} \right] \left[\frac{1 - \sin\rho}{k \sin\rho} \right]^{1/k} \right.\right. \\ &\left.\left. - \zeta_n - \left[\frac{1 - \sin\rho}{k \sin\rho} \right]^{1/k} \sin\psi \right) \sin\delta + \left[\frac{1 - \sin\rho}{k \sin\rho} \right]^{1/k} \cos\psi \cos\delta \right] \end{aligned} \tag{42}$$

where the dilatancy law is expressed by (37).

To approach the study of three-dimensional joints, Eq. (10) must be considered because it defines the reduction angle of the contact.

We must solve the nonlinear equation system that consists of Eqs. (41) and (42) (applied to the entire joint), (3), (10) and the dilatancy law (37). The equations for shear strength can be obtained from this hypothesis. The solution of this system solves the values of the geometrical dilatancy angle δ and instantaneous friction angle ρ, which enable us to calculate the compatible values of the normal and shear force that define the strength of the rock joint.

The geometric locus on an N-T diagram that shows the strength of the rock joint should exclude those values that were obtained for negative values of dilatancy angles and for dilatancy values higher than angle α, which represent the geometrical parameter of the contact (maximum slope of asperities), because these values are physically impossible.

For a null geometrical dilatancy value ($\delta = 0$), Eqs. (41) and (42) show the failure behaviour exactly as predicted by the Hoek and Brown criterion when using a non-associated flow law.

This geometric locus from the modified Hoek and Brown criterion is identified with the second failure mechanism, which corresponds to the developed theoretical formulation. Such a discontinuous shear strength law should intersect with the first failure mechanism (1), which governs the behaviour at low normal stresses. Eq. (1) is applied to all roughness geometries by considering each average contact angle (that is $\alpha_i = \theta_i$).

As indicated above, we must also evaluate the values for m and s while considering the m_0 value, which corresponds to the intact rock, and consider any alterations when applying this value to the conditions of the joint walls according to Eq. (43). The s value can be obtained by means of $s = (m/m_0)^{28/9}$.

When using the Hoek and Brown failure criterion, the value of the instantaneous friction angle depends on the level of stress: as the normal load value increases, a smaller angle value is achieved. Based on previous equations, the second mechanism implies a particular representation of the in-plane stresses $\tau - \sigma$, which depends on the Hoek and Brown parameters. When applied to joints, these parameters

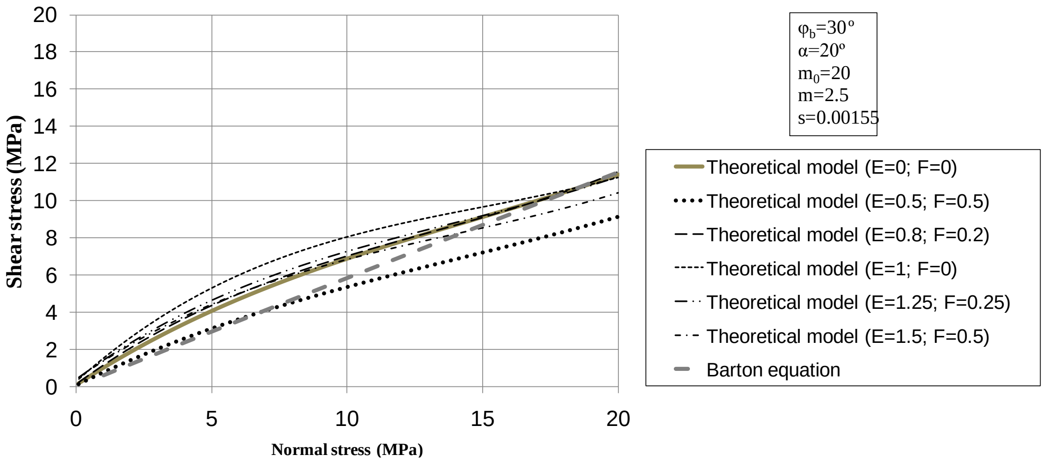

Fig. 8 Shear strength governing law according to the theoretical model (with the modified Hoek and Brown criterion) and experimental Barton model as a function of the E and F parameters that define the dilatancy law for $\varphi_b = 30°$; $\alpha = 20°$; $m_0 = 20$; $m = 2.5$

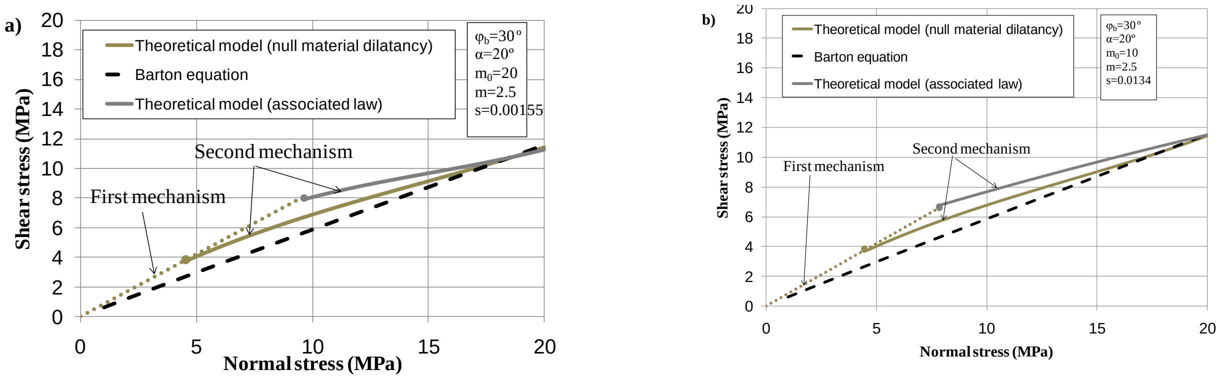

Fig. 9 (a) Shear strength governing law according to the theoretical model (with the Hoek and Brown criterion) and experimental Barton model for $\varphi_b = 30°$, $\alpha = 20°$, $m_0 = 20$, and $m = 2.5$ and (b) shear strength governing law according to the theoretical model (null material dilatancy) and experimental Barton model for $\varphi_b = 30°$, $\alpha = 20°$, $m_0 = 10$, and $m = 2.5$

should include different factors that are difficult to quantify in practice with the criteria that are normally used for rock masses. For joints, alterations can be incorporated if the assigned value of the basic angle φ_b (or residual φ_r) is used to measure these factors. Thus, as predicted by the Barton formula, the value of the peak friction angle that defines the joint shear strength is reduced to the value of the basic angle if the normal stress is equal to the uniaxial compressive strength of the joint wall.

Equalising the value of the basic friction angle with what is predicted by the second failure mechanism for a normal stress on the joint ($\sigma_n = \sigma_c$) and demonstrating that the dilatancy angle is positive enables us to obtain the value of the parameter m according to the Hoek and Brown criterion from the following equation:

$$\varphi_b = (\rho + \kappa_m + \delta)_{\sigma_n = \sigma_c} \tag{43}$$

For null dilatancy, failure at that stress value would be directly indicated by the Hoek and Brown criterion, and we can obtain the value of the parameter m that would produce a shear stress that is equal to $\sigma_c \tan\varphi_b$.

The Hoek and Brown criterion equations can be applied to define the joint strength that corresponds to situations in which solving the second mechanism's equations leads to negative geometric dilatancy angles. Because such angles are not physically possible, such situations require the proposal of null dilatancy and thus a direct application of the failure criterion equations.

6.1.1 Results of the theoretical model with the modified Hoek and Brown criterion

In the most general case, three zones contribute to the strengthening behaviour of a joint that is subjected to shear force (shown in Fig.11(a)):

The first zone corresponds to the first mechanism, which is produced until Eq. (1) is equal to (3).

In the second zone, which involves decreasing geometrical dilatancy values, the second mechanism's equations govern the system until the geometrical dilatancy reaches zero.

Finally, the third zone is described by Eqs. (23) and (24), which correspond to the failure criterion.

In Figs. 8 to 11, the shear strength governing law for some of the values in the theoretical model's parameters are analysed by considering equal three-dimensional roughness areas and the modified Hoek and Brown failure criterion by

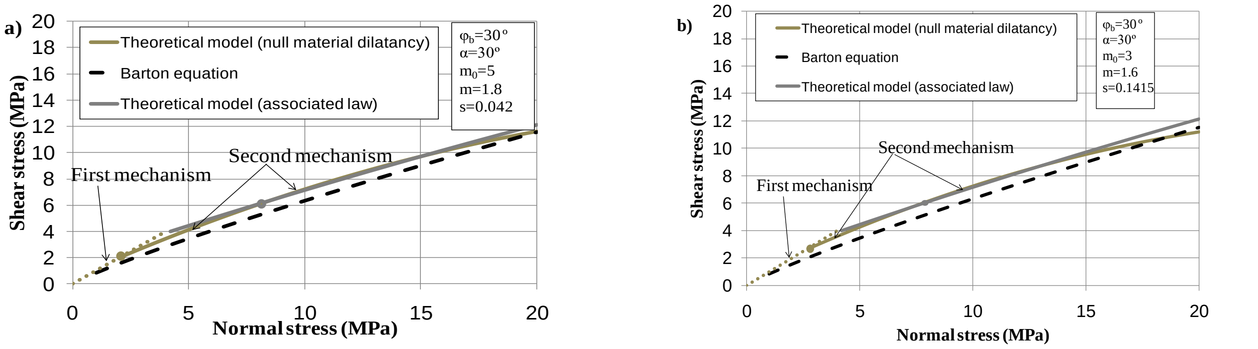

Fig. 10 (a) Shear strength governing law according to the theoretical model (with the Hoek and Brown criterion) and experimental Barton model for $\varphi_b = 30°$, $\alpha = 30°$, $m_0 = 5$, and $m = 1.8$ and (b) shear strength governing law according to the theoretical model (null material dilatancy) and experimental Barton model for $\varphi_b = 30°$, $\alpha = 30°$, $m_0 = 3$, and $m = 1.6$

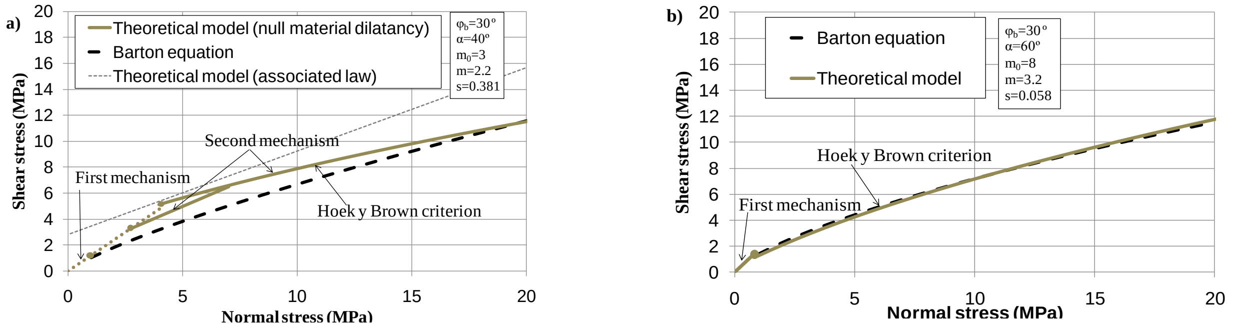

Fig. 11 (a) Shear strength governing law according to the theoretical model (with the Hoek and Brown criterion) and experimental Barton model for $\varphi_b = 30°$, $\alpha = 40°$, $m_0 = 3$, and $m = 2.2$ and (b) shear strength governing law according to the theoretical model (null material dilatancy) and experimental Barton model for $\varphi_b = 30°$, $\alpha = 60°$, $m_0 = 8$, and $m = 3.2$

using a non-associated flow law. These representations also show the shear strength governing law that was deduced when the Barton criterion was applied with the JRC value according to (12). These graphs enable us to compare both models for different values of m_0 and α and a residual friction angle value of 30º in all cases.

As mentioned above, we performed an analysis regarding a non-associated flow law that is represented by the linear law (37) to study rock joints. Thus, the results when evaluating the shear strength of the rock joint on the *N-T* diagram (Fig. 8) show an approximation to Barton´s equation as a function of the *E* and *F* parameters, which define the dilatancy law (37). This figure shows the case that corresponds to a rock joint with a maximum roughness slope α=20°, a residual friction angle value of 30° and a rock mass parameter m_0=20. The result from (43) for the value *m* considers the alteration of the rock mass in the weakness zone from the presence of the joint; this value corresponds to the value for *m*=2.5. The associated flow situation is depicted in the graph for *E*=1 and *F*=0.

According to this graph, the best fit was obtained for *E*=*F*=0, i.e., for zero dilatancy, the curve that represents the strength of the rock joint was very close to the result from Barton's empirical law (5).

This first analysis could be extended to all the analyzed cases. The numerical experimentation indicated that the best non-associated flow law to study the shear strength behaviour of rock joints according to the theoretical model for the failure second mechanism was obtained when using null material dilatancy (Fig. 9 to 11, which only shows the zero dilatancy law and the associated flow law for clarity).

The results with null material dilatancy are quite close to what are predicted by Barton´s law, slightly overestimating the strength at lower average normal stresses, where the peak strength angle is higher than the value that was obtained experimentally.

According to the application of the above equations, these figures show the three zones that delimit the shear strength governing law until a value of 20 MPa is achieved for the uniaxial compressive strength of the joint wall. In Fig. 11(a), the more general case is reached because the three zones of strength appear when null dilatancy is used. The first zone, which is governed by the first mechanism, leads to the zone for the second mechanism, which ends when negatives values of the geometrical dilatancy are obtained (physically impossible values) and then governs the failure criterion when using non-associated flow law. For the associated flow law, the second mechanism disappears because it does not intersect with either the failure criterion or the first mechanism.

The results that were obtained with higher angles for the roughness (Fig. 11(a) and 11(b)) demonstrated that low normal stress values greatly affected the roughness via degradation. In these cases, null geometrical dilatancy was

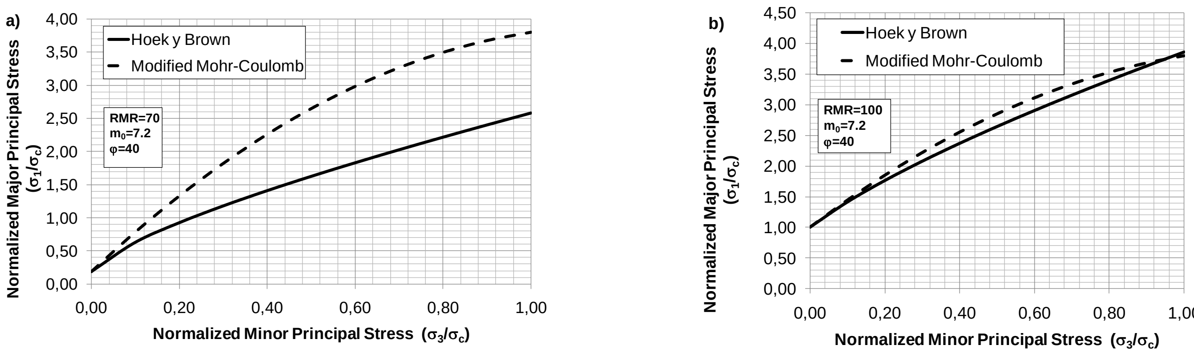

Fig. 12 (a) Comparison of both failure criteria in a $\tau-\sigma$ diagram for GSI≅RMR=70 and (b) Comparison of both failure criteria in a $\tau-\sigma$ diagram for GSI≅RMR =100

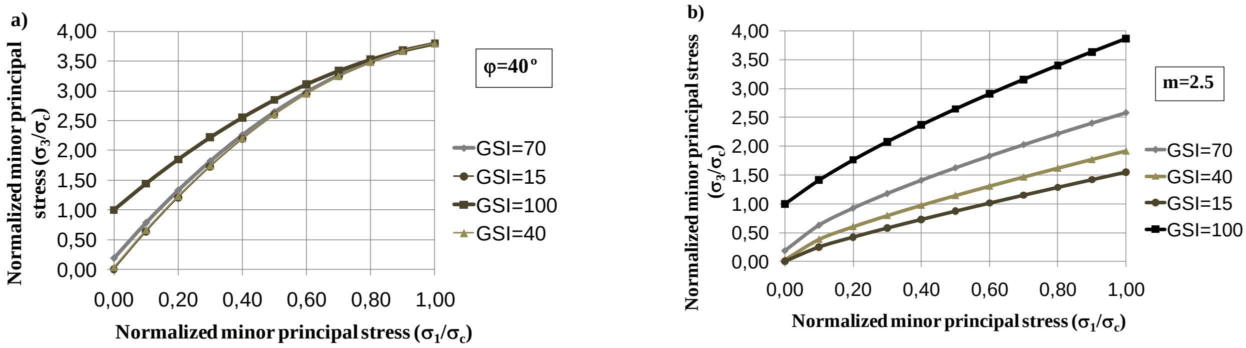

Fig. 13 (a) Influence of the GSI on the modified Mohr-Coulomb criterion for $\varphi = 40°$ and (b) influence of the GSI on the Hoek and Brown criterion for $m = 2.5$

commonly achieved and governed by the rock failure criterion for estimations of joint behaviour. Therefore, these simulations of the roughness with high contact angles corresponded to low-quality rock joints.

At lower roughness angles, the normal load that was applied to the joint had a lower initial effect, although its strength would be lower. Thus, the nonzero geometrical dilatancy zone reached high normal stress values and increased the contribution of the second mechanism.

The consistency of the model is apparent. Variations in the parameter m_0 were almost negligible when considering the values of α and φ_b. The empirical Barton's law was independent of the parameter m_0, although the Hoek and Brown criterion had to use this parameter; thus, Fig. 9(a) and 9(b) used the same value α =20º, while Fig. 10(a) and 10(b) used α =30º was considered when varying the parameter m_0. The consequences of these different values of m_0 in the results of the theoretical model were minimal, as shown in these figures.

6.2 Modified Mohr-Coulomb failure criterion

Following the same approach for the modified Hoek and Brown criterion, stresses in the failure plane for the modified Mohr-Coulomb criterion with a non-associated flow law can be expressed in a parametric form as a function of the instantaneous friction angle (Eqs. (35) and (36)).

Likewise, the following equations for the most realistic case of geometrical modelling with spherical caps can be deduced when considering the axes' rotation expressions to relate normal and shear forces on the middle plane of the joint and its perpendicular with (30) and (31):

$$N_i = \sigma_c a_i \frac{sin^2(\alpha_i-\delta)}{sin^2\alpha_i}\Bigg[\Bigg(1+\frac{r+n_j}{2}-\frac{1}{n_j}\left(\frac{sin\,\rho}{1-sin\,\rho}\right)+\frac{1}{2n_j}\left(\frac{sin\,\rho}{1-sin\,\rho}\right)^2-\left(\frac{r+n_j}{2}-\frac{1}{2n_j}\left(\frac{sin\,\rho}{1-sin\,\rho}\right)^2\right)sin\,\psi\Bigg)cos\,\delta-\left(\frac{r+n_j}{2}-\frac{1}{2n_j}\left(\frac{sin\,\rho}{1-sin\,\rho}\right)^2\right)cos\,\psi\,sin\,\delta\Bigg] \quad (44)$$

$$T_i = \sigma_c a_i \frac{sin^2(\alpha_i-\delta)}{sin^2\alpha_i}\Bigg[\Bigg(1+\frac{r+n_j}{2}-\frac{1}{n_j}\left(\frac{sin\,\rho}{1-sin\,\rho}\right)+\frac{1}{2n_j}\left(\frac{sin\,\rho}{1-sin\,\rho}\right)^2-\left(\frac{r+n_j}{2}-\frac{1}{2n_j}\left(\frac{sin\,\rho}{1-sin\,\rho}\right)^2\right)sin\,\psi\Bigg)sin\,\delta+\left(\frac{r+n_j}{2}-\frac{1}{2n_j}\left(\frac{sin\,\rho}{1-sin\,\rho}\right)^2\right)cos\,\psi\,cos\,\delta\Bigg] \quad (45)$$

where the dilatancy law is expressed by (37).

The nonlinear equation system for Eqs. (44) and (45) (applied to the entire joint), (3), (10) and the dilatancy law (37) produce the geometrical dilatancy angle δ and instantaneous friction angle ρ and enable us to calculate the compatible values of the normal and shear force that define the strength of the rock joint for the second failure mechanism.

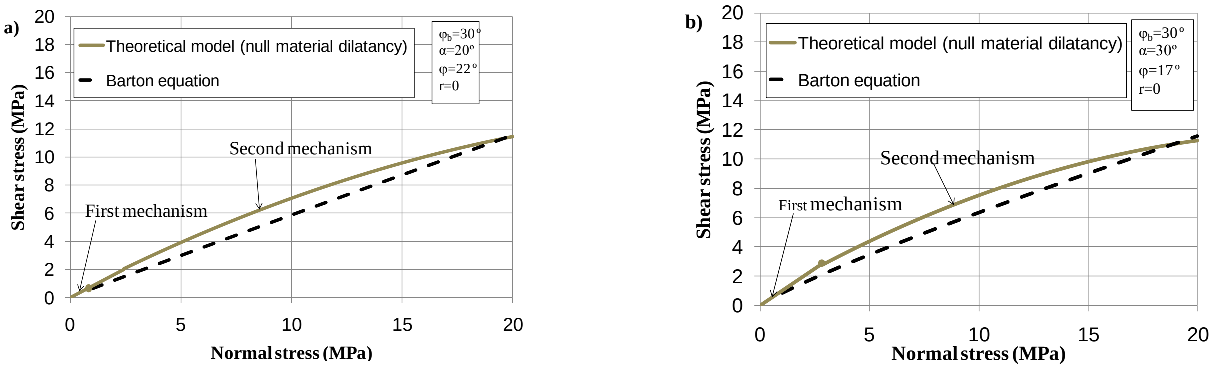

Fig. 15 Shear strength governing law according to the theoretical model (with the modified Mohr-Coulomb criterion) and experimental Barton model for $\varphi_b = 30°$, $\alpha = 20°$, $\varphi = 22°$, and $r = 0$ and (b) shear strength governing law according to the theoretical model (null material dilatancy) and experimental Barton model for $\varphi_b = 30°$, $\alpha = 30°$, $\varphi = 17°$, and $r = 0$

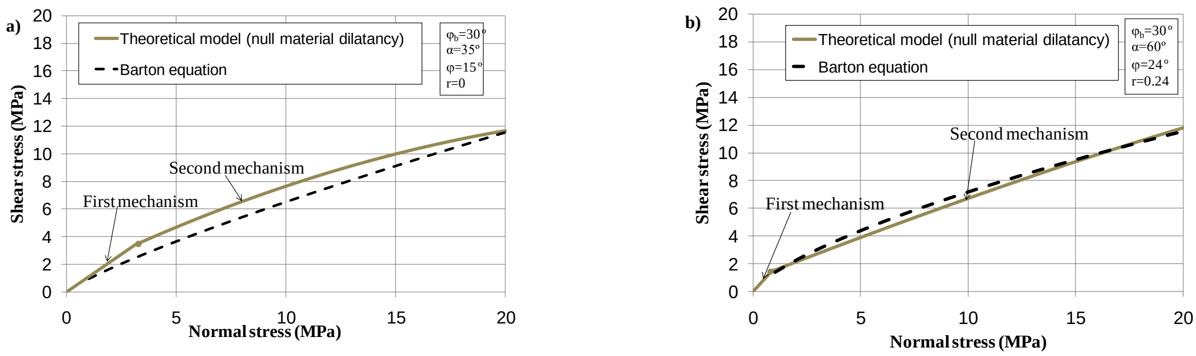

Fig. 16 (a) Shear strength governing law according to the theoretical model (with the modified Mohr-Coulomb criterion) and experimental Barton model for $\varphi_b = 30°$, $\alpha = 35°$, $\varphi = 15°$, and $r = 0$ and (b) shear strength governing law according to the theoretical model (null material dilatancy) and experimental Barton model for $\varphi_b = 30°$, $\alpha = 60°$, $\varphi = 24°$, and $r = 0.24$

An *N-T* diagram can be used to indicate the strength of the rock joint. Negative dilatancy angles and dilatancy values higher than the angle α, which represents the geometrical parameter of the contact (maximum slope of asperities), are physically impossible. This second failure mechanism is limited at low stresses compared to the first failure mechanism.

For a null geometrical dilatancy value ($\delta = 0$), Eqs. (44) and (45) show the failure behaviour exactly as predicted by the modified Mohr-Coulomb criterion when using a non-associated flow law.

When the shear strength of rock joints is studied, the modified Mohr-Coulomb parameters should include different factors that are quantified in practice for rock masses. In this case, the choice of parameters is clear. On the one hand, this study corresponds to a zone that is affected by the discontinuity and therefore altered, so a practically zero value for the parameter *r* can be considered because its influence is negligible when using low values, which errs on the side of safety. On the other hand, the parameter φ can be calculated by using (43), which considers alterability in the rock joint.

6.2.1 Results of the theoretical model with the modified Mohr-Coulomb criterion

Estimating the parameters of this criterion from the Hoek and Brown criterion is intriguing because the Hoek and Brown criterion was introduced long ago and has been provided with a multitude of experimental and field data. In addition, this criterion successfully simulates the most important rock mass failure features, such as the non-linear dependence with stress levels, the influence of the strength and type of rock, and the quality conditions of the rock mass.

Equating the values of the major principal stress for both criteria when no confinement exists ($\sigma_3 \to 0$) can produce the relationship between the parameter s from the Hoek and Brown criterion and the parameter *r* from the non-linear triaxial criterion. Thus, the parameter *r* is associated with the GSI because the parameter *s* depends on this index. This relationship is expressed by the following equation:

$$r = (s)^n \tag{46}$$

where n is the exponent of the modified Hoek and Brown criterion.

Similarly, we can obtain the relationship of the parameter m from the Hoek and Brown criterion with the parameters n_j or φ_j; in this case, the instantaneous friction angles are equal for both criteria in an unconfined situation:

$$\sin \varphi_j = \frac{m}{m + 4r} \tag{47}$$

Eq. (47) shows the conceptual differences between the two criteria and should not be interpreted as a method to obtain the design parameters of a criterion when these factors are known in the other criterion because these parameter values can be obtained outside the usual practice. Thus, for intact rock,

$$sin\,\varphi = \frac{m_0}{m_0 + 4} \tag{48}$$

This equation indicates that the same friction angle value is obtained from the triaxial strength under low confining pressures in intact rock for the same value of the parameter m_0. The value m_0 is associated with a type of rock in the Hoek and Brown criterion; therefore, each rock type is uniquely characterized by a friction angle.

The graph in Fig. 12 shows the result from applying the modified Mohr-Coulomb criterion when considering the equivalence of the above parameters with the modified Hoek and Brown criterion. The strength of the rock joint was much higher when using modified Mohr-Coulomb criterion, primarily because of the significant difference between the two criteria. According to the modified Mohr-Coulomb criterion, a low-quality rock mass is greatly attenuated by the effect of confinement (Fig 13(a)); however, the Hoek and Brown criterion penalizes the degree of alteration and fracturing of a rock mass in all stress levels (Fig. 13(b)). Therefore, as the normal load becomes greater, the different between both failure criteria on the joint becomes more important because the equivalent parameters are obtained under low confining stresses.

Thus, we must obtain the parameters based on specific studies of rock joints to use the modified Mohr-Coulomb criterion and compare it to Barton´s law and therefore to perform a comparison with the Hoek and Brown criterion; in this case, the parameter r was considered null, while the parameter φ was calculated by Eq. (43).

As indicated for the Hoek and Brown criterion, different values of E and F in the dilatancy law (Asadollahi 2009) were used to obtain the best fit to the experimental data. Fig. 14 shows the values E and F for roughness angles of α=20° and φ_b=30º, which obtained the best results for null dilatancy. In Figs. 15 and 16, only the results for null dilatancy are shown.

In Figs. 14 to 16, the shear strength governing law for some of the values in the theoretical model parameters were analysed by considering equal three-dimensional roughness areas and the modified Mohr-Coulomb failure criterion by using a non-associated flow law. These representations also showed the shear strength governing law that was deduced when Barton's law was applied with the JRC value according to (12). These graphs enable us to compare both models for different values of α and a residual friction angle value of 30º in all cases.

As observed in the depicted graphs, an associated flow law produced higher values than those from Barton's method for this study's theoretical model.

As with the Hoek and Brown criterion, the results with null material dilatancy were quite close to what was predicted by Barton's law, slightly overestimating the strength at lower average normal stresses.

According to the application of the above equations, these figures show the three zones that delimit the shear strength governing law until a value of 20 MPa is achieved for the uniaxial compressive strength of the joint wall. The first zone, which is governed by the first mechanism, leads to the zone of the second mechanism, which ends when negatives values of the geometrical dilatancy are obtained (physically impossible values), and then governs the failure criterion by using a non-associated flow law.

The results with higher roughness angles indicate a low-quality rock mass because this model requires a low friction angle parameter. In Fig. 16(b), null geometric dilatancy was obtained for the second mechanism, so the modified Mohr-Coulomb criterion was applied directly (a nonzero value of the parameter r was used only in this case), which produced very close values to what were predicted by the experimental formulation, although these values were slightly lower.

At lower roughness angles, the nonzero dilatancy zone achieved high values of normal stress and increased the contribution of the second mechanism.

The surface roughness could be studied similarly for both criteria, as suggested geometrically in section 4. Linear joints do not optimally represent three-dimensional behaviour, so we cannot obtain reasonable values with the modified Hoek and Brown or modified Mohr-Coulomb criteria when determining a roughness failure mechanism, mainly because linear joint models, such as the saw-tooth or circumference arc models, imply a greater contact area between the contact surfaces and overestimate the peak strength above both realistic values and the values that are obtained for three-dimensional geometries. Consequently, null dilatancy situations appear very easily in almost all ranges of parameters that are assigned to the model, which reduces the study to the first mechanism and the failure criterion. Thus, these studies cannot represent situations of dilatancy via asperity failure.

7. Conclusions

This research established a theoretical formulation to elaborate the criteria of shear strength for rock discontinuities. The results were compared to empirical equations, producing very close values for different roughness states.

Two failure mechanisms were identified in accordance with a normal load level on the joint. Both mechanisms had clear physical interpretations and were supported by empirical evidence that was collected in numerous studies. The first mechanism appeared for low normal stresses and corresponded to slippage between the faces of each joint wall. When the acting normal stress was high, the second failure mechanism occurs, which corresponds to a failure of contacts because of the plastification of the roughness. Both mechanisms were theoretically analysed, and their behaviour followed equations (1) and (3).

As indicated by the theoretical formulation for the analysis of the second mechanism, the rock joints must be adequately characterized based on the choice of roughness models with a realistic appropriate failure criterion and must consider both the geometrical dilatancy that is produced by the breakage of contacts according to a calculated direction and non-associated flow laws.

The influence of the surface roughness was characterised by defining simple geometric parameters. In particular, the average contact angle θ for the roughness was calculated. This value is easily measurable in both the field and the laboratory and is defined as the angle for which the tangent is the roughness height divided by the half-length at the mid-plane, which is covered by the surface roughness. Different assumed roughness geometries were characterised by using this parameter. In particular, the use of irregularities such as spherical caps on the joint mid-plane is recommended for the three-dimensional study of joints.

The modified Hoek and Brown and modified Mohr-Coulomb criteria were used in this research. These criteria enabled us to obtain very different behaviours for altered or fractured rock masses. In this case, the modified Mohr-Coulomb criterion largely depended on the confining stress, losing its influence after alteration or for a low-quality rock mass when the confinement pressure increased (unlike the Hoek and Brown criterion). This fact makes this criterion useless to compare what occurs in joints under high stresses by the direct transformation of parameters between both criteria because this transformation occurs at low stresses.

The parameters were chosen so that the results of Barton´s law could associate a residual strength angle to a normal stress that equalled the uniaxial strength of the joint. For the modified Mohr-Coulomb criterion, a value for the parameter s that equals zero is suggested.

A linear law of dilatancy (37) was used to assess the importance of non-associated flow, so the best results were obtained for null material dilatancy, which considered significant changes for soft rock masses or altered zones of weakness.

Very close results with respect to the empirical values (Barton´s equation) were obtained by using asperities of angles from 20º to 60º, which enhanced the predictions by the theoretical model for the second mechanism with respect to the associated flow case.

The theoretical formula that was presented herein could be used to study the shear strength of rock joints based on non-empirical assumptions with a relatively simple and practical analysis process.

References

Alejano, L.R. and Alonso E. (2005), "Considerations of the dilatancy angle of rocks and rock masses", *Int. J. Rock Mech. Sci. Geomech. Abstr*., **42**(4), 481-487. https://doi.org/10.1016/j.ijrmms.2005.01.003.

Archambault, G., Roleau, A., Daigneault, R. and Flamand, R. (1993), "Progresive failure of rock masses by a self similar anastomosing process of rupture at all scales and its scale effects on their shear strength", *Proceedings of the 2nd International Workshop on Scale Effects in Rock Masses*, Lisboa, Portugal, June.

Asadollahi, P. (2009), "Stability analysis of a single three dimensional rock block: effect of dilatancy and high-velocity water jet impact", Ph.D. Dissertation, University of Texas, Austin, Texas, U.S.A.

Barton, N. (1973), "Review of a new shear strength criterion for rock joints", *Eng. Geol*., **7**, 287-332. https://doi.org/10.1016/0013-7952(73)90013-6.

Barton, N. and Bandis, S. (1982), "Effects of block size on the shear behavior of jointed rock", *Proceedings of the 23rd US Symposium on Rock Mechanics*, Berkeley, California, U.S.A., August.

Belem, T. (2016), "Quantitative parameters of primary roughness for describing the morphology of surface discontinuities at various scales ", *Geomech. Eng*., **11**(4), 515- 530. https://doi.org/10.12989/gae.2016.11.4.515.

Belem, T., Souley, M. and Homand F. (2007), "Modelling surface rougness degradation of rock joint wall during monotonic and cyclic shearing", *Acta Geotech*., **2**(4), 227-248. https://doi.org/10.1007/s11440-007-0039-7.

Chong, S., Kim, J., Cho, G. and Song, K. (2020), "Preliminary numerical study on long-wavelength wave propagation in a jointed rock mass", *Geomech. Eng*., **21**(3), 227- 236. https://doi.org/10.12989/gae.2020.21.3.227.

Fairhurst, C. (2003), "Stress determination in rock: A brief history and review", *Int. J. Rock Mech. Min. Sci*., **40**(7-8), 957-973. https://doi.org/10.1016/j.ijrmms.2003.07.002.

Gens, A., Carol, I. and Alonso, E.E. (1990), "A constitutive model for rock joints, formulation and numerical implementation", *Comput. Geotech.* **9**, 3-20. https://doi.org/10.1016/0266-352X(90)90026-R.

Grasselli, G. and Egger, P. (2003), "Constitutive law for the shear strength of rock joints based on three-dimensional surface parameters", *Int. J. Rock Mech. Min. Sci*., **40**(1), 25-40. https://doi.org/10.1016/S1365-1609(02)00101-6.

Heuze, F.E. and Barbour, T.G. (1982) "New models for rock joints and interfaces", *J. Geotech. Eng. Div*., **108**(5), 757-76. https://doi.org/10.1061/(ASCE)0733-9410(1983)109:7(1011).

Hoek, E. and Brown, E.T. (1997), "Practical estimates of rock mass strength", *Int. J. Rock Mech. Sci. Geomec. Abstr*., **34**(8), 1165-1187. https://doi.org/10.1016/S1365-1609(97)80069-X.

Hoek, E., Carranza-Torres, C. and Corkum B. (2002), "Hoek-Brown failure criterion – 2002 Edition", *Proceedings of the NARMS-TAC 2002, Mining Innovation and Technology*, Toronto, Canada, July.

Hoek, E., Marinos, P. and Benissi, M. (1998), "Applicability of the geological strength index (GSI) classification for weak and sheared rock masses; The case of the Athens schist formation", *B. Eng. Geol. Environ*., **57**(2), 151-160. https://doi.org/10.1007/s100640050031.

Hu, W. and Lin, H. (2018), "Non-linear shear strength criterion for a rock joint with consideration of friction variation", *Geotech. Geol. Eng*., **36**(6), 3731-3741. https://doi.org/10.1007/s10706-018-0567-y.

Huang, S.L., Oelfke, S.M. and Speck, R.C. (1992), "Applicability of fractal characterization and modelling to rock joint profile", *Int. J. Rock Mech. Min. Sci*., **29**, 89-98. https://doi.org/10.1016/0148-9062(92)92120-2.

Jaeger, J.C. (1971), "Friction of rocks and stability of rock slopes", *Geotecnique* **21**(2), 97-34. https://doi.org/10.1680/geot.1971.21.2.97.

Ladanyi, B. and Archambault, G. (1969), "Simulations of the shear behavior of a jointed rock mass", *Proceedings of the 11th US Symposium on Rock Mechanics*, Berkeley, California, U.S.A. June.

Lee, Y.H., Carr, J.R., Barr, D.J. and Haas, C.J. (1990), "The fractal dimension as a measure of the roughness of rock discontinuity profiles", *Int. J. Rock Mech. Min. Sci*., **27**, 453-464. https://doi.org/10.1016/0148-9062(90)90998-H.

Leichnitz, W. (1985), "Mechanical properties of rock joints", *Int. J. Rock Mech. Min. Sci*., **22**(5), 313-321. https://doi.org/10.1016/0148-9062(85)92063-7.

Lin, H., Hu, W., Chen, Y., Cao, R., Wang, Y., Yong, R. and Du, S.

(2020), "Shear resistance of rock joint under nonuniform normal stress", *Adv. Mater. Sci. Eng.*, 1-8. https://doi.org/10.1155/2020/9316482.
Muralha, J. (1995), *Fractal Dimension of Joint Roughness Surfaces*, Balkema, Rotterdam, The Netherlands.
Patton, F.D. (1966), "Multiple modes of shear failure in rock", *Proceedings of the 1st Congress of International Society of Rock Mechanics*, Lisboa, Portugal, September.
Plesha, M.E. (1987), "Constitutive models for rock discontinuities with dilatancy and surface degradation", *Int. J. Numer. Anal. Meth. Geomech.*, **11**(4), 345-362. https://doi.org/10.1002/nag.1610110404.
Qiu, X., Plesha, M.E, Huang, X. and Haimson, B.C. (1993), "An investigation of the mechanics of rock joints-part II: Analytical investigation", *Int. J. Rock Mech. Min. Sci.*, **30**(3), 271-287. https://doi.org/10.1016/0148-9062(93)92730-E.
Saeb, S. and Amadei, B. (1992), "Modeling rock joints under shear and normal loading", *Int. J. Rock Mech. Min. Sci.*, **29**(3), 267-278. https://doi.org/10.1016/0148-9062(92)93660-C.
Samadhiya, N.K., Viladkar, M.N. and Al-Obaydi, M.A. (2008) "Three-dimensional joint/interface element for rough undulating major discontinuities in rock masses", *Int. J. Geomech.*, **8**(6), 327-335. https://doi.org/10.1061/(ASCE)1532-3641(2008)8:6(327).
Schneider, H.J. (1976), "The friction and deformation behavior of rock joints", *Rock Mech. Rock Eng.*, **8**(3), 169-184. https://doi.org/10.1007/BF01239813.
Serrano, A. and Olalla, C. (1994), "Ultimate bearing capacity of rock masses", *Int. J. Rock Mech. Min. Sci.*, **31**(2), 93-106. https://doi.org/10.1016/0148-9062(94)92799-5.
Serrano, A., Olalla, C. and Galindo, R.A. (2014), "Micromechanical basis for shear strength of rock discontinuities", *Int. J. Rock Mech. Min Sci.*, **70**, 33-46. https://doi.org/10.1016/j.ijrmms.2014.02.021.
Serrano, A., Olalla, C. and Gonzalez, J. (2000), "Ultimate bearing capacity of rock masses based on the modified Hoek-Brown criterion", *Int. J. Rock Mech. Min. Sci.*, **37**(6), 1013-1018. https://doi.org/10.1016/S1365-1609(00)00028-9.
Singh, M., Raj, A. and Singh, B. (2011), "Modified Mohr-Coulomb criterion for non-linear triaxial and polyaxial strength of intact rocks", *Int. J. Rock Mech. Min. Sci.*, **48**(4), 546-555. https://doi.org/10.1016/j.ijrmms.2011.02.004.
Singh, M. and Singh, B. (2012), "Modified Moh-Coulomb criterion for non-linear triaxial and polyaxial strength of jointed rocks", *Int. J. Rock Mech. Min. Sci.*, **51**, 43-52. https://doi.org/10.1016/j.ijrmms.2011.12.007.
Tse, R. and Cruden, D.M. (1979), "Estimating joint roughness coefficients", *Int. J. Rock Mech. Min. Sci.*, **16**(5), 303-307. https://doi.org/10.1016/0148-9062(79)90241-9.
Veermer, P.A and De Borst, R. (1984), "Non-associated plasticity for soils, concrete and rock", *Heron*, **29**(3). https://doi.org/10.1016/0148-9062(79)90241-9.
Xie, H., Wang, J.A. and Kwasniewski, M.A. (1999), "Multifractal characterization of rock fracture surfaces", *Int. J. Rock Mech. Min. Sci.*, **36**, 19-27. https://doi.org/10.1016/S0148-9062(98)00172-7.
Zhang, X., Yi, B., Jiang, Q., Feng, X. and Chen, N. (2017), "Evaluation models for the peak shear-strength and shear-resistance components of rough rock joints", *J. Test. Eval.*, **45**(6), 20170134. https://doi.org/10.1520/JTE20170134.
Zhao, L., Jiao, K., Zuo, S., Yu, C. and Tang, G. (2020), "Pseudo-static stability analysis of wedges based on the nonlinear Barton-Bandis failure criterion", *Geomech. Eng.*, **20**(4), 287-297. https://doi.org/10.12989/gae.2020.20.4.287.

JS